Inorganic Chemistry

Article

pubs.acs.org/IC

DFT Investigation of the Molybdenum Cofactor in Periplasmic Nitrate Reductases: Structure of the Mo(V) EPR-Active Species

Frédéric Biaso,* Bénédicte Burlat, and Bruno Guigliarelli

Unité de Bioénergétique et Ingénierie des Protéines, UMR 7281, Centre National de la Recherche Scientifique, Institut de Microbiologie de la Méditerranée, and Aix-Marseille University, 31 Chemin Joseph Aiguier, 13402 Marseille Cedex 20, France

Supporting Information

ABSTRACT: The periplasmic nitrate reductase NAP belongs to the DMSO reductase family that regroups molybdoenzymes housing a bis-molybdopterin cofactor as the active site. Several forms of the Mo(V) state, an intermediate redox state in the catalytic cycle of the enzyme, have been evidenced by EPR spectroscopy under various conditions, but their structure and catalytic relevance are not fully understood. On the basis of structural data available from the literature, we built several models that reproduce the first coordination sphere of the molybdenum cofactor and used DFT methods to make magneto-structural correlations on EPR-detected species. "High-*g*" states, which are the most abundant Mo(V) species, are characterized by a low-anisotropy ***g*** tensor and a high g_{min} value. We assign this signature to a six-sulfur coordination sphere in a pseudotrigonal prismatic geometry with a partial disulfide bond. The "very high-*g*" species is well described with a sulfido ion as the sixth ligand. The "low-*g*" signal can be successfully associated to a Mo(V) sulfite−oxidase-type active site with only one pterin moiety coordinated to the molybdenum ion with an oxo or sulfido axial ligand. For all these species we investigate their catalytic activity using a thermodynamic point of view on the molybdenum coordination sphere. Beyond the periplasmic nitrate reductase case, this work provides useful magneto-structural correlations to characterize EPR-detected species in mononuclear molybdoenzymes.

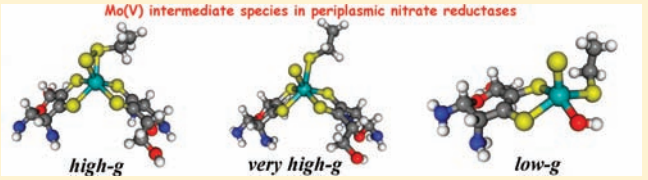

1. INTRODUCTION

Mononuclear molybdoenzymes are oxidoreductases which metabolize a wide diversity of small inorganic substrates (nitrate, formate, sulfur, or arsenic compounds). Usually this large family of enzymes is categorized in three structural subclasses: the sulfite oxidase (SO), xanthine oxidase (XO), and dimethyl sulfoxide reductase (DMSOR) families.[1] Within each of the three families the molybdenum cofactor (Moco) exhibits a peculiar structure: the metal is coordinated to either one or two pyranopterins, and in most enzymes an additional amino acid which can be serine, cysteine, seleno-cysteine, or aspartic acid is present in the coordination sphere.[2,3] Moreover, some additional oxygen or sulfur ligands arising from the oxo or sulfido group, hydroxide ion, or water molecule are observed. Within the DMSOR family, which is essentially composed of enzymes from prokaryotic organisms, nitrate reductases reduce nitrate to nitrite by a two-electron and two-proton transfer reaction thanks to a Mo−bis(molybdopterin) cofactor (Scheme 1). These enzymes are believed to play an essential role in the biological cycle of nitrogen and have been extensively studied during the last decades by many biophysical techniques (EPR spectroscopy, electrochemistry, extended X-ray absorption fine structure spectroscopy, Raman spectroscopy, X-ray crystallography) to investigate the structural and redox behavior of the molybdenum cofactor and understand the catalytic mechanism.[3−18] In this mechanism the Mo ion is considered to cycle between the +IV, +V, and +VI oxidation states, but the structure of the different intermediates involved in the enzyme cycle is still largely debated.[10,19−23] Periplasmic nitrate reductases (NAP) constitute a subgroup of the DMSOR family which can be monomeric (NapA)[21,24,25] or dimeric (NapAB).[9,24,26−29] All of them possess a catalytic subunit harboring the Moco and an electron transfer [4Fe-4S] center. Several crystallographic studies of NAP enzymes have been performed and reveal different structures of the Moco depending on the microorganism and crystallization conditions[9,21,25,26,30] (Scheme 2). A common feature is the coordination of the Mo atom by two pterin groups and by a

Scheme 1. Structure of the Molybdenum Cofactor of Periplasmic Nitrate Reductases[a]

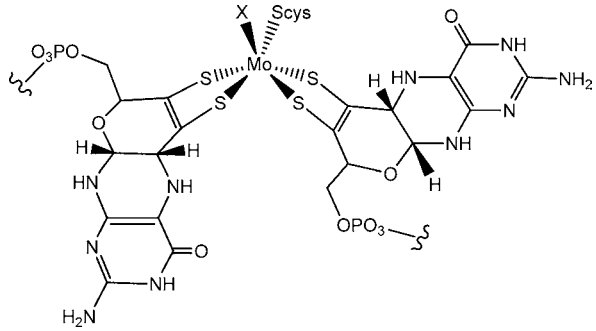

[a]X represents an exogenous ligand (H_2O, OH^-, NO_3^-, O^{2-},...).

Received: July 19, 2011
Published: March 7, 2012

Scheme 2. Molybdenum Coordination Modes Proposed from Crystallographic Structures of Periplasmic Nitrate Reductases[a]

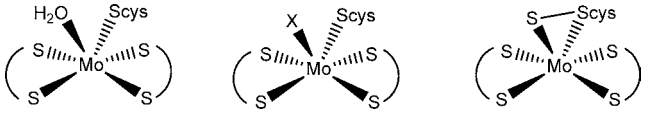

[a]PDB codes: 2NYA from *Escherichia coli* (left), 1OGY from *Rhodobacter sphaeroides* (middle), 2V3V from *Desulfovibrio desulfuricans* (right). X stands for an unresolved ligand.

thiol from cysteine, but one can notice the diversity of the small ligand proposed in the Mo coordination sphere which suggests a high plasticity of the active site related to its ability to bind various anions. Depending on the study, this ligand was proposed to be an oxygen atom from a water, hydroxo, or oxo group[21,25] or a sulfido group which can be bound to the sulfur atom of the Cys ligand.[26,30] Since in most of these studies the crystals were prepared in aerobic conditions, the molybdenum ion is usually considered to be in the +VI oxidation state.[21,25]

However, it is worth noting that even in the oxidized state of NAP several Mo(V) species were evidenced by EPR. The biological role of Mo(V) intermediates is a crucial question since it can constitute an essential part of the catalytic cycle.[31] Despite extensive investigations, the catalytic relevance of the corresponding species is still not established and although their magnetic parameters are well known their structures remain elusive. Moreover, for as-prepared NAP samples, the Mo(V) EPR signal intensity can be largely substoichiometric representing from 2.5% to 60% of the total molybdenum content depending on the preparation and bacterial origin.[10] These heterogeneities demonstrate the versatility of the system and are a source of complexity for functional studies. Usually, on the basis of the Mo(V) *g* values, NAP EPR signals are classified into three main groups: "high-*g*" species which correspond to the major species and "low-*g*" and "very high-*g*" species (Figure 1 and Table 1). In addition, hyperfine couplings (*hfc*) with one or more magnetic nuclei are detected by EPR spectroscopy on NAP (Table 1) and reveal the presence of exchangeable or nonexchangeable protons in the vicinity of the Mo atom. As explained hereafter, the proportions of each signal are strongly dependent on the redox treatment undergone by the enzyme, on the presence of redox mediators, or on incubation with substrate. As the electronic ***g*** and hyperfine coupling ***A*** tensors are expected to be highly sensitive to the environment of the metal ion, this diversity of EPR signatures suggests a great variability of the structure of the molybdenum cofactor.

In order to understand the relationships between the various three-dimensional structures proposed for the Mo cofactor in periplasmic nitrate reductases and the EPR-detected Mo(V) species, we present in this work a theoretical analysis of their magnetic parameters. DFT calculations, including geometry optimization and determination of spectroscopic parameters, have been performed on different kind of models of NAP molybdenum cofactor with the aim of deducing some magneto-structural correlations for EPR-detected species. We emphasize results for the so-called "high-*g*" signals which are the major components of molybdenum paramagnetic forms in NAP. On the basis of thermodynamic calculations, we present also an interpretation of the catalytic relevance of the proposed structures as a function of the oxidation state of the metal.

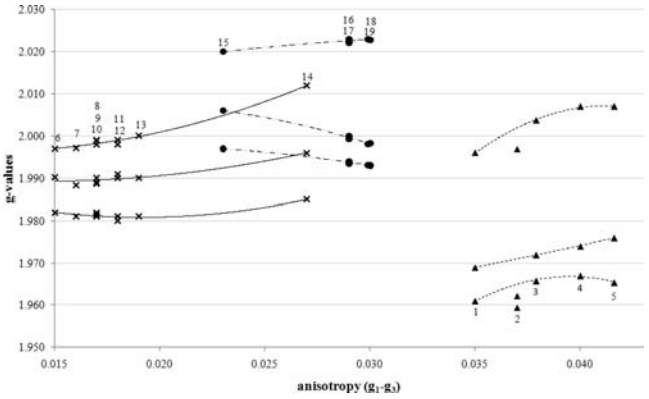

Figure 1. Plot of the *g* values of the Mo(V) species against anisotropy for several bacterial and eukaryotic molybdenum enzymes. Numbers correspond to the following signals: (1) *Pp* NapAB "low-*g* split",[58] (2) *Pp* NapAB "low-*g* unsplit",[61] (3) *Chicken* SO "low pH",[100] (4) *Pp* SoxCD "low pH",[101] (5) *At* SO "low pH",[102] (6) *Ss* NarB "high-*g* resting",[67] (7) *Ec* NapA "high-*g* resting",[21] (8) *Pp* NapAB "high-*g* nitrate",[61] (9) *Dd* NapA "high-*g* turnover",[30] (10) *Av* NAS "high-*g* nitrate",[66] (11) *Pp* NapAB "high-*g* resting",[58] (12) *Rs* and *Sg* NapAB "high-*g* resting",[24,60] (13) *Dd* NapA "high-*g* nitrate",[63] (14) *Dd* FDH "high-*g* resting",[69] (15) *Mf* FDH "very high *g*",[68] (16) *Pp* NapAB "very high *g*",[61] (17) *Rs* NapAB "very high *g*" (this work), (18) *Av* NAS "very high *g*",[66] and (19) *Ss* NarB "very high *g*".[67] Symbols (●, ×, ▲) have been chosen to classify signals by resemblance. *At, Arabidopsis thaliana*; *Av, Azotobacter vinelandii*; *Dd, Desulfovibrio desulfuricans*; *Ec, Escherichia coli*; *Mf, Methanobacterium formicicum*; *Pp, Paracoccus pantotrophus*; *Rs, Rhodobacter sphaeroides*; *Sg, Shewanella gelidimarina*; *Ss, Synechococcus species*; FDH, formate dehydrogenase; NAR, respiratory nitrate reductase; NAS, assimilatory nitrate reductase.

These results clarify the role of the EPR-detected Mo(V) state from a structural and a mechanistic point of view.

2. METHODS

The structural models used in this study are built from molybdenum cofactor Cartesian coordinates of published NAP crystallographic structures (PDB codes 2NYA,[21] 2NAP,[25] 2V3V,[30] 1SOX,[32] 1OGY[9]). Molybdopterins and cysteine residue are truncated to simplify studies without significant loss of accuracy in electronic and magnetic properties calculations: pterin moieties are modeled by their first heterocycle and chelated dithiolene functions, whereas the cysteine chain is modeled by an ethanethiolate fragment. Geometry optimizations and frequency calculations of molybdenum cofactor models were performed in the gas phase with the Gaussian03 program package (ver. E.01)[33] using the B3LYP hybrid functional (Becke's three-parameter hybrid exchange functional with 20% of Hartree−Fock admixture and the Lee−Yang−Parr nonlocal correlation functional)[34,35] and SDD basis set with d function for sulfur and effective core potentials for molybdenum.[36] The SDD basis set was chosen for optimization because of its good ability to model second-row transition-metal complexes.[37] Energy minima were characterized with harmonic frequency calculations (no imaginary frequencies). The electronic properties and magnetic constants were obtained with the ORCA package (ver. 2.8)[38] by running single-point calculations on fully or partially optimized structures. The ORCA program uses the coupled-perturbed self-consistent field (CP-SCF) formalism.[39] These single-point calculations were carried out at the B3LYP level of theory with the zero-order regular approximation (ZORA) for relativistic components.[40,41] Mo and S were represented by the all-electron TZV-ZORA basis set,[42] and C, H, N, and O were represented by the all-electron SV-ZORA basis set[42] with Ahlrichs polarization functions.[43] Our calculation utilizes the empirical van der Waals correction implemented in the ORCA program.[44] The S^2 expectation value for unrestricted Kohn−Sham wave functions

dx.doi.org/10.1021/ic201533p | *Inorg. Chem.* 2012, 51, 3409−3419

Table 1. Experimental EPR Parameters of Mo(V) Species in Periplasmic Nitrate Reductase[a]

source	signals	g_1	g_2	g_3	g_{av}	anisotropy $g_1 - g_3$	rhombicity $(g_1 - g_2)/(g_1 - g_3)$	$A_{ii}(^1H)$ [MHz]	ref
Ec NapA	high *g*	1.997	1.988	1.981	1.989	0.016	0.56	16.8, 13.4, 13.4	21
Rs NapAB	high-*g* resting	1.999	1.991	1.981	1.990	0.018	0.45	17.1, 15.7, 14.0, 8.1, n.d., n.d.[c]	9,60
Rs NapA	high-*g* resting	1.998	1.991	1.981	1.990	0.018	0.44	17.6, 15.1, 14.0[c]	59
Pp NapAB	high-*g* resting	1.998	1.990	1.981	1.990	0.018	0.46	17.9, 14.6, 14.0, 7.8, n.d., n.d.	58
Sg NapAB	high-*g* resting	1.998	1.990	1.981	1.990	0.018	0.46	17.9, 14.6, 5.4	24
Dd NapA	high-*g* nitrate	2.000	1.990	1.981	1.990	0.019	0.53	12.9, 14.0, 12.9[d]	63
Pp NapAB	high-*g* nitrate	1.999	1.989	1.981	1.990	0.017	0.59	17.9, 12.0, 12.9, 9.0, n.d., n.d.	61
Dd NapA	high-*g* turnover	1.999	1.990	1.982	1.990	0.017	0.53	16.2, 18.2, 15.4[e]	30
Rs NapAB	very high *g*	2.023	2.000	1.994	2.006	0.029	0.79	21.8, 19.9, 16.8	*c*
Pp NapAB	very high *g*	2.022	1.999	1.993	2.005	0.029	0.80	20.7, 20.7, 18.5	61
Pp NapAB	low *g* (split)	1.996	1.969	1.961	1.975	0.035	0.77	36.4, 38.1, 42.8[b]	58
Pp NapAB	low *g* (unsplit)	1.997	1.962	1.959	1.973	0.037	0.93		61

[a]Since *g* values are close to 2.0, *hfc* constants have been translated into frequency units using 1 mT = 28 MHz. [b]For one exchangeable proton. [c]This work (simulations performed by using the EasySpin free package[103]). [d]For one nonexchangeable proton. [e]For two exchangeable protons.

(which is a good spin contamination indicator) has been checked for each single-point calculation and does not exhibit significant deviations from the ideal value (i.e., 0.75 for Mo(V) systems). Some recent studies have demonstrated the ability of DFT methods with a hybrid functional like B3LYP to properly reproduce EPR parameters of several transition-metal compounds and, in particular, Mo(V) complexes.[45−51] One can also notice their excellent ratio accuracy/calculation time. To test the validity of our method for the molybdenum cofactor of NAP which possesses a high content of sulfur atom in the Mo coordination sphere, we performed preliminary calculations on well-characterized molybdenum−sulfur synthetic complexes with known structural and magnetic properties (see Supporting Information). These tests confirm the good ability of B3LYP to estimate the *g* values of molybdenum complexes. Nevertheless, we find the well-known tendency of this hybrid density functional with 20% exact Hartree−Fock exchange admixture to slightly overestimate the g_1 value and the ***g***-tensor anisotropy for Mo(V) six-coordinate complexes.[45,52−54] In some cases, in vacuo optimizations are not well suited to model active sites of enzymes. Indeed, neglecting the proteic environment can be a source of errors in geometrical optimizations. When in vacuo full optimizations led to large geometrical deviations from the crystal structure, we used partial optimizations by keeping constant some bond distances and angles around the metal in order to mimic protein constraints

3. RESULTS AND DISCUSSION

EPR spectroscopy has long been used to characterize the Mo cofactor in the NAP family (Table 1). In Figure 1 are collected the *g* values of the Mo(V) species detected in monomeric and dimeric NAP and in structurally related enzymes like cytoplasmic assimilatory nitrate reductases (NAS) or formate dehydrogenases (FDH), the cysteine ligand of the Mo ion being replaced with a seleno−cysteine in the latter. The *g* values are plotted as a function of the ***g***-tensor anisotropy, a representation that is well adapted to emphasize structural correlations between various paramagnetic species.[55−57] Three groups of correlated species clearly appear that include the "low-*g*", "high-*g*", and "very high-*g*" species, respectively. This indicates that within each group the Mo ion has the same coordination sphere, the ***g***-tensor variations being due to a change of the ligand field strength (for instance, upon Cys to Se-Cys ligand replacement) or to small structural modifications (angle or distance bonds) induced by changes of the second coordination sphere of the metal or of its close environment.

In order to correlate structural and magnetic data, we calculated the ***g*** and ***A*** tensors for several Mo(V) models based on the NAP crystallographic data. The 3 × 3 electronic ***g*** tensor was obtained from the sum of four contributions: the free electron *g* value (g_e), the relativistic mass correction (RMC), the diamagnetic gauge correction (GC), and the second-order cross terms between the orbital Zeeman (OZ) and spin−orbit coupling (SOC) operators. Equation 1 describes the matrix element g_{ij} of the electronic ***g*** tensor

$$g_{ij} = g_e\delta_{ij} + \Delta g_{ij}^{\mathrm{RMC}} + \Delta g_{ij}^{\mathrm{GC}} + \Delta g_{ij}^{\mathrm{OZ/SOC}} \quad (1)$$

For transition-metal-containing species, the main contribution is $\Delta g_{ij}^{\mathrm{OZ/SOC}}$ which strongly depends on the nature and relative energy positions of frontier orbitals.[39] Since this major contribution cannot exactly be calculated, the accuracy of the calculation depends on the method of approximation. The ORCA software uses the spin−orbit mean-field approach (SOMF) to estimate the SOC operator.[50] Given that the major contributions of *g* values arise from spin−orbit coupling of the metal and the coordinated atoms, we focused on the first coordination sphere of the molybdenum ion. The 3 × 3 *hfc* ***A*** tensor results from the interaction between the unpaired electron and a magnetic nucleus *N*. The complete expression of the *hfc* matrix element A_{ij} can be written as

$$A_{ij}(N) = T_{ij}(N) + T_{ij,\mathrm{orb}}(N) + \delta_{ij}(A_{\mathrm{FC}}(N) + A_{\mathrm{PC}}(N)) \quad (2)$$

where $T_{ij}(N)$ and $T_{ij,\mathrm{orb}}(N)$ are the first- and second-order terms of the anisotropic dipolar interaction, respectively. $A_{\mathrm{FC}}(N)$ corresponds to the isotropic Fermi contact interaction (first order term), and $A_{\mathrm{PC}}(N)$ is the isotropic pseudocontact interaction (second order term). δ_{ij} are values of the identity matrix. As for the ***g*** tensor, the *hfc* tensor second-order terms depend on the SOC contributions which may introduce some inaccuracy. Fortunately, the SOC correction is negligible for light atoms like protons. Thus, in our study, the main source of error results from calculation of the spin density at the position of nucleus *N* which strongly affects the $A_{ij}(N)$ values (for more details on DFT calculations of this interaction, see refs 46 and 51). Moreover, it must be kept in mind that geometry optimizations of Mo(V) models do not directly take into account the protein environment which induces steric constraints on bond lengths and angles. Thus, EPR parameter calculations must be used carefully and only with a qualitative approach based on comparison within model series.

For the sake of clarity, we presented separately in the following text the results concerning the different types of Mo(V)

dx.doi.org/10.1021/ic201533p | Inorg. Chem. 2012, 51, 3409−3419

Scheme 3. Tested Mo(V) Models for "High-*g*" Species[a]

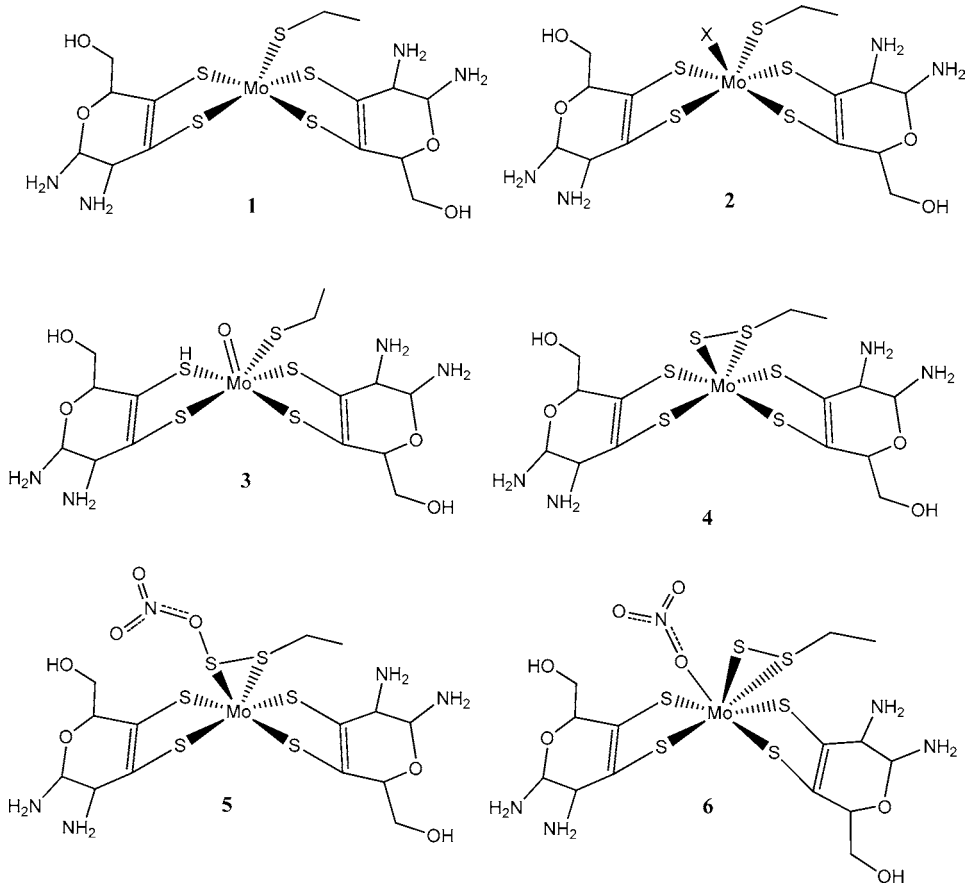

[a]The X atom of model 2 stands for H_2O, O^{2-}, S^{2-}, OH^-, SH^-, or NO_3^-.

signals of the NAP enzymes, namely, the "high-*g*", "very high-*g*", and "low-*g*" EPR signals.

3.1. "High-*g*" Species. The "high-*g*" family (Figure 1) contains the most common and most intense signals of Mo(V) EPR-detected species in NAP enzymes. All "high-*g*" signals are characterized by a rhombic ***g*** tensor and *hfc* interactions with two $I = 1/2$ nuclei (Table 1). The "high-*g*" signals can be further subdivided according to the anisotropy and the rhombicity of the ***g*** tensor. This group is composed of three kinds of signatures called "resting", "nitrate", and "turnover". "High-*g* resting" signal is characterized by a ***g***-tensor rhombicity of about 0.45, this value rising to 0.53 in "high-*g* nitrate" and "high-*g* turnover" signals. The "high-*g* resting" (or "high-*g* split") signal is usually observed in as-prepared NAP samples from *Pp*, *Rs*, and, recently, *Sg*.[9,24,58−60] Its intensity depends on enzyme preparations[10] and varies, for instance, between 3% and 20% of the total molybdenum content for *Rs* NapAB and up to 70% for *Rs* NapA. In the presence of nitrate and using dithionite as a reductant, this signature is replaced by the "high-*g* nitrate" signal in *Pp*[61] and *Rs*[62] NapAB. This signal has also been obtained under reductive conditions in the absence of substrate in *Ec*[21] and with or without substrate in *Dd* NapA samples,[63] suggesting that this species might not be a nitrate-bound form.[21] When methyl viologen was used as a reductant and in the presence of nitrate, the Mo(V) signature is characterized by the so-called "high-*g* turnover" signal,[30,63] but to date, this signal was reported in *Dd* NapA samples only. Moreover, while the detected *hfc* interactions are related to nonexchangeable protons in "high-*g* resting" and "high-*g* nitrate" signals,[9,61,63] they were proposed to arise from two exchangeable protons in "high-*g* turnover".[63] However, the strong resemblance of EPR parameters between all these signals suggests that the Mo coordination is the same for these species with only subtle structural differences in the vicinity of the molybdenum center.

Interestingly, the "high-*g*" signals are very different from those given by enzymes of the XO and SO family which contain monopterin active sites. In particular, their *g* values are higher, which probably reflects significant $\Delta g_{ij}^{OZ/SOC}$ sulfur contributions and are in agreement with the presence of the two pterins coordinated to the Mo(V) ion. Moreover, the experimental *hfc* constants with two nonexchangeable protons were analyzed by ^{1}H ENDOR spectroscopy[64] (Table 1) and could be attributed to the β-CH_2 protons of the coordinating cysteine, the magnitude of the hyperfine coupling being consistent with the presence of protons at two or three bond distances from the metal.

Considering these experimental results, we used NAP crystal structures (PDB codes 2NYA, 1OGY, and 2V3V) to construct active site models with two pterins and one cysteine and with or without additional ligands (Scheme 3). Model **1** is the simplest case with a pentacoordinated structure. Models **2** are equivalent to the common structures found in crystallographic studies in which the coordination sphere of the molybdenum ion is completed with a sixth ligand. For these models, we tested the most probable anions or molecules that could bind to the metal: H_2O, OH^-, O^{2-}, NO_3^-, SH^-, S^{2-}. Model **3** derives from models **2** and has been tested to investigate the effect of pterin protonation.[65] Models **4** and **5** possess a sulfur

dx.doi.org/10.1021/ic201533p | *Inorg. Chem.* 2012, 51, 3409−3419

ion which makes a partial disulfide bond with the cysteine ligand. This side-on η^2 arrangement has been recently proposed[26,30] and could protect the molybdenum atom from any direct attack of the solvent. In the case of an associative inner-sphere mechanism, Mo(V) intermediates would have a seven-coordinated geometry.[20] Thus, we studied model **6**, which possess a seven-coordinate geometry with a nitrate ion.

Geometry optimizations of models **1**−**6** imply large modifications in bonds and angles around the metal compared with the crystal structure. The absence of surrounding protein in our models can explain these structural modifications as the geometry around the molybdenum must be constrained by electronic and steric interactions with close amino acids. EPR parameters of the optimized structure of models **1**−**6** have been determined and reported in the Supporting Information. In fact, these EPR parameters are significantly different from the experimental values measured for "high-*g*" signals. Nevertheless, these calculated EPR parameters could be used for studying magneto-structural correlations. To our knowledge, no molybdoenzyme or mononuclear Mo(V) complex with a rhombic ***g*** tensor and g_{min} values larger than 1.98 have been reported in the literature excepted for NAP (Table 1), NAS,[66,67] and FDH[68,69] active sites[70] (Figure 1). All enzymes possess two pterins, one cysteine or selenocysteine, and probably an additional unknown ligand coordinated to the molybdenum ion. Among good candidates for an additional ligand, the oxo ion is one of the most proposed in the literature since EXAFS experiments indicate the presence of Mo═O bonds in the Mo(VI) state of NAP samples.[61] Our attempts to find the geometry of model $\mathbf{2O^{2-}}$ which has a ***g*** tensor in good agreement with the "high-*g*" species failed even when some geometrical constraints were used (see Supporting Information). Interestingly, comparison of *g* values of optimized models **1**−**6** reveals that only structures with six sulfur atoms around the metal give $g_{min} \geq 1.98$ (models $\mathbf{2SH^-}$, **4**, and **5**). This suggests that the large g_{min} value for the "high-*g*" Mo(V) species is an indicator of the presence of six sulfur (or selenium) atoms in the first coordination sphere. On the other hand, the model $\mathbf{2S^{2-}}$ has a $g_{min} = 1.897$ that indicates the great sensitivity of the ***g*** tensor to structural variations and emphasizes the necessity of deeper investigations on six sulfur-coordinated Mo(V) systems (named $[MoS_6]$ thereafter).

Thus, we investigated the influence of structural parameters on working models considering a $[MoS_6]$ structure as the most probable coordination sphere for the "high-*g*" species. Among all structural parameters, *g* values are very sensitive to those related to the first coordination sphere, especially the dihedral angle between the four sulfur of the pterin dithiolene ligands which is known as the Bailar twist[71] (θ in Scheme 4). In the second coordination sphere, a well-known structural determinant of the Mo(V) ***g*** tensor in molybdenum complexes is the dithiolene fold angle which is the angle between the plane formed by the Mo−S dithiolene bonds and the plane formed by the dithiolene ligand (Scheme 4).[52,72−74] In the case of periplasmic nitrate reductases, the crystallographic structures show that these dithiolene fold angles are small (<10°). Moreover, in optimized models of this study these fold angles remain close to zero (see Supporting Information). Then, in all cases the calculations of EPR parameters were performed on a cofactor structure characterized by small values of the dithiolene fold angles.

Scheme 4. Schematic View of the Molybdenum Coordination Sphere for Dihedral Angles θ = 0° (left) and 60° (right)

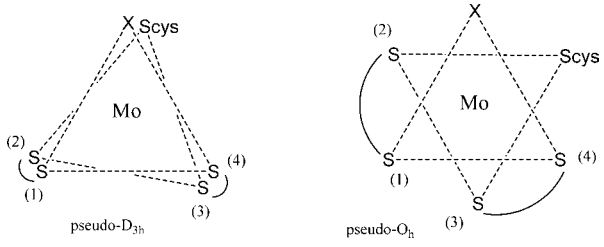

Thus, the Bailar twist was the main geometrical parameter investigated for "high-*g*" models. For models $\mathbf{2SH^-}$, $\mathbf{2S^{2-}}$, **4**, and **5** with six sulfur ligands, significant variations of the Bailar twist were observed between optimized geometries (see Supporting Information). This angle variation is associated to the rotation of the ligands around the C_3 axis. In fact, an increase of this angle can be seen as an indication of a deformation of the pseudo-D_{3h} symmetry toward D_3 (pseudo-octahedral symmetry). This enhancement of the O_h character is associated to a rotation of one pterin out of the plane containing the molybdenum ion and the other pterin. The main reason for this rotation is the presence of the exogenous ligand. Steric and electronic repulsions induced by the ligand cause a shift of the cysteine ligand toward one pterin that leads to rotation of the pterin to minimize constraint. This effect is more pronounced for optimized models in which the exogenous ligand is strongly charged. Model $\mathbf{2S^{2-}}$ has a Bailar twist of $\theta = 53°$, whereas models **4** and **5** display a Bailar twist of $\theta = -10°$ and $-16°$, respectively. The minimal rotation of one pterin is then observed for models **4** and **5**, which have a pseudo-D_{3h} symmetry. For these latter models, the partial disulfide bond plays a crucial role in ligand organization around the metal.

To give better insight into the correlation between the Bailar twist, the molecular orbitals, and the ***g*** tensor of $[MoS_6]$ complexes, we studied the two typical symmetry cases of a tris-dithiolene Mo(V) compound: the trigonal prismatic symmetry (D_{3h}, $\theta = 0°$) and the distorted D_3 geometry (O_h in local symmetry and D_3 in global symmetry, $\theta = 60°$). Electronic properties of these models have been already studied by DFT,[75] and we propose here an insight of the EPR parameters with the interpretation of the *g* values with regard to the molecular orbitals. All calculation results have been reported in the Supporting Information. The study of these two models suggests that "high-*g*" species which have low-anisotropy ***g*** tensors correspond to pseudo-D_{3h} systems with some distortions toward D_3 geometry.

These first results on optimized models suggest that the trigonal prismatic geometry is favored by the presence of a pseudo-disulfide bond, in contrast with models with the oxo ligand which lead to an electronic preference for distorted octahedral structures.[76] Then models **4** and **5** appear to be the best candidates corresponding to a $[MoS_6]$ coordination sphere with pseudo-trigonal prismatic geometry. In order to take into account the constraints and interactions of the proteic environment on the active site, we performed EPR properties calculations on a partially optimized model **4** deduced from the *Dd* NapA crystal structure (PDB code 2V3V), which was modeled with a disulfide bond in a side-on η^2 coordination. This structure possesses a Bailar angle of $\theta = 14°$, which corresponds to a trigonal prismatic geometry with a rather small twist of pterins toward the octahedral symmetry and thus is in agreement with magneto-structural correlations proposed for "high-*g*" species. The twisted trigonal prismatic geometry has already been proposed for intermediate species during the oxygen

dx.doi.org/10.1021/ic201533p | Inorg. Chem. 2012, 51, 3409−3419

atom transfer mechanism in the DMSOR.[77,78] Crystallographic atomic coordinates have been frozen for all non-hydrogen atoms (i.e., geometry optimization concerns only hydrogen atoms). However, given the fact that for a crystallographic resolution of 2.0 Å the standard deviation of coordinates can be estimated to be about 0.2 Å,[79] we studied the evolution of g values by considering a possible variation of a few percent in bond lengths between the Mo ion and the ligands. In order to avoid deformations toward D_3 symmetry caused by elongation of only one part of coordination bond lengths, all Mo−S bond lengths have been modified by the same ratio from 95% to 110% of crystallographic values, and only the hydrogen positions were optimized (Figure 2).

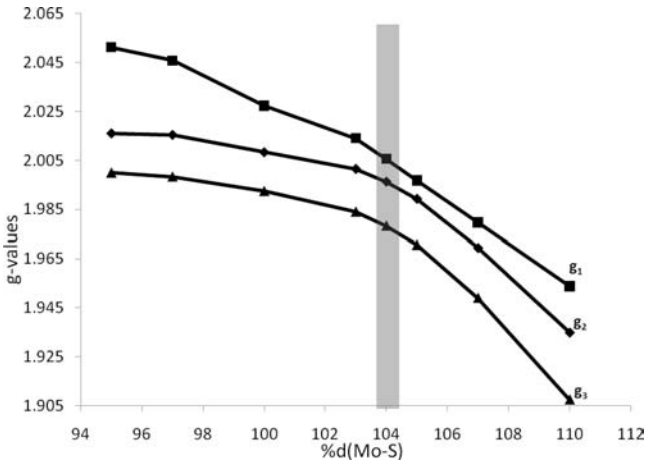

Figure 2. Dependence of g values with Mo−S bond length for the "2V3V model". Reference (100%) corresponds to the value for crystallographic geometry. Gray box indicates the best fit for "high-g" signals.

Figure 2 shows that the g values are significantly affected by Mo−S distances. Increasing lengths between the metal ion and ligands leads to a decrease of the g values, whereas the $\boldsymbol{g}$-tensor anisotropy and rhombicity are roughly conserved. This can be explained by the decrease of spin density delocalization on ligands when sulfur atoms (which give positive Δg contributions) are moved away from the molybdenum center. Finally, the best fit we obtained for g values of "high-g" species corresponds to model **4** with crystallographic coordinates and an increase of Mo−S bonds of 4% (≅0.1 Å). This small deviation of bond lengths is close to the uncertainties on atomic positions due to the resolution of the crystallographic structure. This partially optimized model (named "**4_2v3v**") is 26 kcal/mol higher in energy than the fully optimized model **4** (in vacuum), which can be balanced by the steric and electrostatic effects of the protein environment and small reorientations of bonds as already shown in other enzymes. Indeed, some very large strain energies have already been calculated for proteins by comparison of QM and QM/MM methods. For example, Torrent et al. calculated an energy difference of 47 kcal/mol for the methane monooxygenase active site due to rotation of ligands.[80] In the case of NAP, several aromatic residues (Trp-622, Phe-689, Tyr-713 in the 2V3V X-ray structure) are located in the vicinity of Moco and interact by π interactions with pterin moieties which likely result in constraints in the cofactor structure and limit the reorientation of the ligands. The model "**4_2v3v**" has the following g values: $g_1 = 2.006$, $g_2 = 1.996$, $g_3 = 1.978$. The resulting anisotropy of the $\boldsymbol{g}$ tensor is 0.027, which is significantly small for Mo(V) signals, as is the case for "high-g" species. Interestingly, the greatest *hfc* constants are related to ^{1}H of the cysteine β-CH_2 group ($A_{xx} = 3.9$, $A_{yy} = 4.2$, $A_{zz} = 8.7$ MHz) as already proposed from the study of the hyperfine splitting observed in "high-g" signals.[61] The non-negligible deviation between calculated and experimental *hfc* values is likely due to a different orientation of the ethanethiolate group modeling the cysteine ligand which can also be influenced by the proteic constraints. Indeed, by modifying the dihedral angle between the disulfide bond and the C−C bond of the ethanethiolate ligand we can improve the ^{1}H *hfc* values of the β-CH_2 group without a significant change of energy (less than 1 kcal/mol) and g values (see the angular variation of the ethyl group in the Supporting Information). For a SSCC dihedral angle value of 75° we obtain a ^{1}H *hfc* of $A_{xx} = 6.6$, $A_{yy} = 6.7$, $A_{zz} = 11.0$ MHz. Although the ^{1}H *hfc* is well known to be strongly sensitive to the basis set, using EPR-II or TZVP instead of SVP basis set does not give a significant change (<10% of variation) in the calculated values.

As we have previously seen, the "high-g" term groups three different species: "high-g resting", "high-g nitrate", and "high-g turnover". The differences between these signals are tiny in terms of magnetic parameters and behavior. This suggests that there are no significant differences in the first coordination sphere of Mo(V). Then, we propose a common structure for all these species based on a six-sulfur coordination sphere with a partial disulfide bond in a side-on η^2 fashion which gives a pseudo-trigonal prismatic geometry. These species can be strongly related to the crystal structure proposed by Najmudin et al.[30] Differences between "resting", "nitrate", and "turnover" signals could be due to the presence of ions or solvent molecules not directly coordinated to the molybdenum center but in its close neighborhood or to a rearrangement of the proximal amino acids surrounding the Moco leading to small variations of its magnetic properties.

3.2. "Very High-g" Species. "Very high-g" signals have only been detected for some enzymes of the DMSO reductase family. These signatures could be observed alone in as-prepared samples of cytoplasmic assimilatory nitrate reductases (NAS)[66,67] or in recent as-prepared preparations of NAP from *Rs* in which the "very high-g" signal was observed together with the "high-g resting" signal and accounted for only a few percent.[59] These kinds of signals were also observed with FDH[68] or polysulfide reductase (PSR)[81] samples treated with excess dithionite or substrate and with NAP samples treated with dithionite, cyanide, or azide and subsequently oxidized by air, nitrate, or ferricyanide.[58,61,63] On the other hand, Jepson et al. have shown that addition of dithionite to *Synechococcus sp.* NarB (a NAS type enzyme) samples leads to conversion from "very high-g" to "high-g" signatures. After consumption of reductants, the NAS samples partially return to the "very high-g" signal.[66,67] All these observations may reflect a complex redox behavior and ask whether "high-g" and "very high-g" species have a redox relationship. The unusually large g values characterizing the "very high-g" Mo(V) species (Table 1) suggest a significant delocalization of the spin density on the sulfur atoms which suppose, as for "high-g" species, that only a [MoS_6] coordination sphere with a pseudo-trigonal prismatic geometry can give this kind of $\boldsymbol{g}$ tensor for molybdoenzyme active sites. Concerning *hfc* interactions, like most of the NAP Mo(V) signatures, the "very high-g" signal is split by a coupling with one nonexchangeable $I = 1/2$ nucleus.[58]

To reproduce these EPR parameters, we used models with six sulfur atoms in the first coordination sphere of the molybdenum

dx.doi.org/10.1021/ic201533p | Inorg. Chem. 2012, 51, 3409−3419

Table 2. Mo(V) EPR Parameters of the "High-*g*", "Very High-*g*", and "Low-*g*" Mo(V) Species and Our Proposed Models[a]

	g_1	g_2	g_3	anisotropy $g_1 - g_3$	rhombicity $(g_1 - g_2)/(g_1 - g_3)$	$A_{ii}(^1H)$ (in MHz)
Rs "high-*g* resting"	1.999	1.991	1.981	0.018	0.45	17.1, 15.7, 14.0
model "**4_2v3v**"	2.006	1.996	1.978	0.027	0.34	3.9, 4.2, 8.7
Rs "very high *g*"	2.023	2.000	1.994	0.029	0.79	21.8, 19.9, 16.8
model "**2S^{2-}_2v3v**"	2.025	2.005	1.995	0.030	0.67	−1.7, −2.6, 3.8
Pp "low-*g* split"	1.996	1.969	1.961	0.035	0.77	36.4, 38.1, 42.8
model **7**	1.995	1.973	1.967	0.028	0.79	39.7, 42.0, 59.1
model **9**	1.992	1.967	1.961	0.031	0.81	41.6, 43.6, 60.8

Scheme 5. Tested Mo(V) Models for "Low-*g*" Species

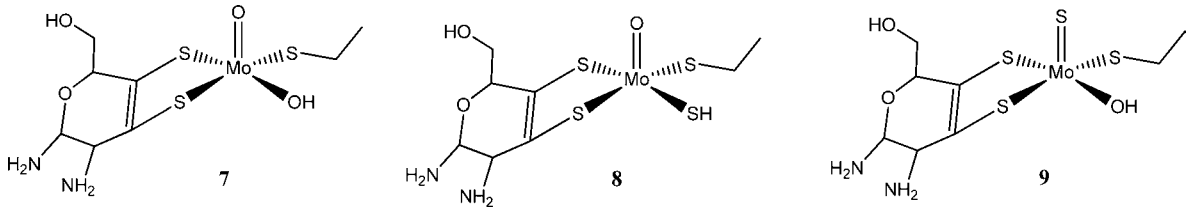

center. Obviously, EPR signatures demonstrate that in both species the metal must have a +V formal oxidation state, and it is well known that sulfur-based ligands are noninnocent ligands and can play an important role in the redox chemistry of the active site.[82] On the basis of the hypothesis that neither cysteine residue nor pterin moieties can be oxidized or reduced without irreversible damages, we supposed that the disulfide bond could be the redox-active part of the "high-*g*"/"very high-*g*" conversion. Model **2S^{2-}** is two-electron more reduced than model **4** and can be a good candidate to describe a redox-related form of "high-*g*" species.[83] As previously described for the "high-*g*" models, we have taken into account the protein environment by starting from crystal coordinates (2V3V) and frozen positions of all non-hydrogen atoms except the disulfide bond between the cysteine residue and the sixth sulfur atom. In other words, this partial optimization keeps the bis-molybdopterin atom positions as in the crystal structure. Moreover, we considered a total charge of −2 for this model, which means a more reduced state than the "high-*g*" model. This model has been named "**2S^{2-}_2v3v**" in the following text. The main modifications caused by addition of electrons include breaking the partial disulfide bond (the S−S distance increases from 2.407 Å for 2V3V crystal structure to 3.257 Å for the partially optimized model) and a significant lengthening of the Mo−S_{cys} bond (from 2.368 to 2.772 Å). In contrast with the fully optimized model **2S^{2-}**, this "pseudo-crystallographic" geometry shows only very small deformations toward D_3 symmetry without a major increase of the electronic energy (28 kcal/mol compared to the optimized structure of model **2S^{2-}** in vacuum). Obviously, calculated EPR properties (g_1 = 2.025, g_2 = 2.005, g_3 = 1.995) are strongly affected by these structural modifications and show a good agreement with "very high-*g*" signals (Table 2). As it has been supposed, the sulfur atoms contribute largely to the *g* shifts, especially the exogenous sixth sulfur. This is related to the important delocalization of the spin density onto the ligands with only 42% on the molybdenum atom. As for the "high-*g*" species, the largest *hfc* constants are obtained for the ^{1}H nuclei of the cysteine β-CH_2 group (A_{xx} = −1.7, A_{yy} = −2.6, A_{zz} = 3.8 MHz) but the significant deviation between the experimental and the calculated *hfc* values likely results from a different orientation of the ethyl group modeling the cysteine residue. For a SSCC dihedral angle value of 20° we obtain a ^{1}H *hfc* of A_{xx} = 7.3, A_{yy} = 7.8, A_{zz} = 9.6 MHz (see the angular variation of the ethyl group in the Supporting Information).

3.3. "Low-*g*" Species. "Low-*g*" signals could be observed in NapAB from *P. pantotrophus* when the enzyme was incubated with dithionite in the absence of substrate (nonturnover conditions).[58,61] The corresponding electronic ***g*** tensor is nearly axial (Table 1), and in some enzyme preparations a proportion of the "low-*g*" signal is split by a I = 1/2 nucleus and was therefore called "low-*g* split". This splitting was not present when the sample was prepared in deuterated buffer and attributed to a proton of a weakly bound water molecule or hydroxide ion.[58] The "low-*g*" NAP signals resemble the signature of "rapid type I" XO species (g_1 = 1.989, g_2 = 1.970, g_3 = 1.966),[84] and they can be successfully correlated with the signature of the "low-pH" SO species (Figure 1). Enzymes of the SO and XO families possess a molybdenum cofactor with only one pterin, one or two oxo groups, and a sulfur-based ligand (cysteine for SO, HS^-, for XO). As a consequence, this similarity in magnetic properties has been interpreted as a dissociation of one pterin ligand from the Mo ion,[58,61] leading to a square pyramidal geometry with one pterin, a cysteine, and two exogenous ligands. A DFT study of the "low-pH" SO signal has been published recently, and a model with an oxo ion in the axial position and an equatorial hydroxide ion has been proposed (model **7** in Scheme 5).[85] Since calculated magnetic parameters of this model are in good agreement with "low-pH" SO species, it can also be a suitable model for "low-*g* split" NAP signal. Nevertheless, considering the current discussion on the oxygen/sulfur atom in the molybdenum coordination sphere, we studied further models with a sulfur-based exogenous ligand. With the aim of determining whether an exogenous sulfur ligand can be present in the molybdenum coordination sphere of "low-*g*" NAP species, we performed geometry optimization on models **7**−**9** (Scheme 5) based on the Moco's structure of one of the best resolved crystallographic structures of SO (PDB code 1SOX). Model **7** corresponds to the "low-pH" SO proposed structure with an oxo and a hydroxide ligand. In model **8** the hydroxide ligand is replaced by a SH^- ion, whereas in model **9** the oxo ligand is replaced by a sulfido ion. The calculated *g* values for the optimized structures of models **7**−**9** have been reported in Table 3. In these models

dx.doi.org/10.1021/ic201533p | *Inorg. Chem.* 2012, 51, 3409−3419

Table 3. Calculated EPR Parameters of the Optimized Structure of "Low-*g*" Models 7−9

model	g_1	g_2	g_3	anisotropy $g_1 - g_3$	rhombicity $(g_1 - g_2)/(g_1 - g_3)$	$A_{ii}(^1H)$ (in MHz)[a]
7	1.995	1.973	1.967	0.028	0.79	39.7, 42.0, 59.1
8	2.030	1.979	1.975	0.055	0.93	21.0, 28.0, 22.0
9	1.992	1.967	1.961	0.031	0.81	41.6, 43.6, 60.8

Scheme 6. Schematic Representation of Proposed Structures of the Active Site of "High-*g*" (left), "Very High-*g*" (middle), and "Low-*g*" (right) Species[a]

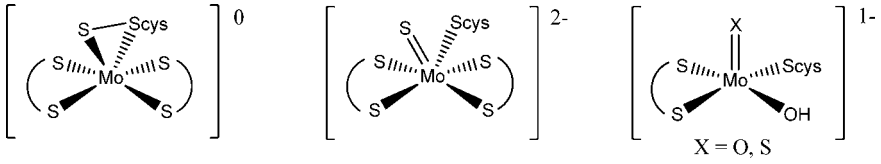

[a]X stands for O or S.

we notice that the optimized geometry remains close to the 1SOX sulfite oxidase crystal structure without significant deviation in atomic position except the expected bond lengthening when an oxygen atom is replaced by a sulfur atom. For models **7** and **9**, the calculated *g* values are in good agreement with those of the "low-*g*" signals. Because of a large g_1 value the ***g*** tensor is strongly anisotropic for model **8**. Investigations on $\Delta g_{ij}^{OZ/SOC}$ contributions reveal that the axial ligand has no significant weight in *g* values as compared to the equatorial one. Thus, the oxygen/sulfur replacement induces a too large g_{max} value when it is made on the equatorial position. This electronic effect explains why models **7** and **9**, the structures of which are only distinguished by the axial ligand, possess *g* values close to "low-*g*" ones. For model **7** we find similar EPR parameters to the ones published[85] with a slightly better agreement with the experimental values of "low-*g*" NAP signals. For both models **7** and **9** the major part of the spin density is localized in the Mo-d_{xy} orbital, in good agreement with the proposed value for "low-pH" SO,[86] and the *hfc* constants $A_{ij}(^1H)$ calculated for the hydroxide proton (Table 3) correspond qualitatively to the experimental values ("low-*g* split") with a large isotropic component (spin density in the s_H orbital). A second significant *hfc* constant appears in these models with one β-CH_2 proton of the cysteine. Nevertheless, this splitting is too small to be easily observed experimentally by EPR and could be hidden by the peak line width.

Since calculated magnetic parameters fit correctly the experimental ones, we conclude that models **7** and **9** (optimized geometry) inspired from the sulfite oxidase molybdenum cofactor structure provide a good electronic description for "low-*g* split" species. Although the EPR parameters of "low-*g* split" NAP species resemble those for "low-pH" SO and "rapid-type I" XO signals, our DFT results suggest that a sulfur-based ligand can be present in the molybdenum coordination sphere in the axial position. Considering the similarity of the two "low-*g*" signals, we suggest that "low-*g* unsplit" species have an active site structure close to optimized models **7** and **9** (*g* values of the other model do not match experimental ones). The difference of ^1H *hfc* magnitude between the "split" and the "unsplit" signals could be due to the position of the hydroxide proton since the proton spin density (and consequently ^1H *hfc* constant) is strongly affected by its orientation relative to the Mo−O bond. Such position could be locked by the presence of a hydrogen bond with neighboring amino acids or hydroxide or water molecule as proposed for the "high-pH" SO species.[87]

In conclusion, the structures we propose for "high-*g*", "very high-*g*", and "low-*g*" NAP species are recapitulated in Scheme 6, and the corresponding calculated EPR parameters are compiled in Table 2.

3.4. Catalytic Relevance of Mo(V) Species. Among all Mo(V) EPR species detected so far in NAP enzymes, only the species from the "high-*g*" family were considered as putative catalytic intermediates. "Low-*g*" species have long been suspected to arise from a "damaged" active site. Calculations show indeed that in this species the binding of one pterin is lost but the coordination of the cysteine and possibly of the exogenous sulfido ligands are maintained. These signals represent only a few percent of total molybdenum and replace the "high-*g* resting" species after prolonged incubation upon reductive conditions. Whereas the "low-*g*" species has certainly no catalytic relevance, it has been shown that a strong redox treatment results in the reappearance of the "high-*g* resting" signal,[61] which suggests that displacement of one pterin could be a reversible process.

Recently, Fourmond et al.[10] have shown that the "high-*g* resting" state observed in as-prepared enzyme from *Rs* is a dead end in the catalytic cycle that can be activated by a reduction process followed by a slow and an irreversible reaction (irreversible activation process). It remains unclear why the main part of the enzyme is inactive and what the nature of the chemical transformation during this activation process is. Since nitrate needs two electrons from the active site to be reduced, it has long been proposed that the substrate binds the metal ion in the most reduced form (Mo^{IV}). In a recent study, Cerqueira et al. proposed that the approach of the substrate toward the active site proceeds in two steps using the disulfide-bridged structure as an active species.[20] In that scenario, the first step consists of the linkage of the nitrate ion on the sulfido exogenous ligand followed by a shift of the SS_{cys} moiety and decoordination of the cysteine to give direct access to the metal for the substrate (Scheme 7). From calculations of transition state energies, these authors proposed that in the NAP catalytic mechanism the substrate coordinates preferentially on the fully oxidized molybdenum (Mo^{VI}). On the other hand, using energy calculations, two recent studies proposed a catalytic mechanism in which the nitrate binds to the molybdenum in the +IV oxidation state.[19,88] In order to understand the influence of the molybdenum oxidation state on the nitrate binding, we studied the stability of the Mo−S_{cys} bond which must be broken during the "sulfur-shift" mechanism. For this purpose, we used model **5**, which

dx.doi.org/10.1021/ic201533p | Inorg. Chem. 2012, 51, 3409−3419

Scheme 7. "Sulfur-Shift"-Based Mechanism for Nitrate Coordination on the Molybdenum Center (adapted from ref[20])

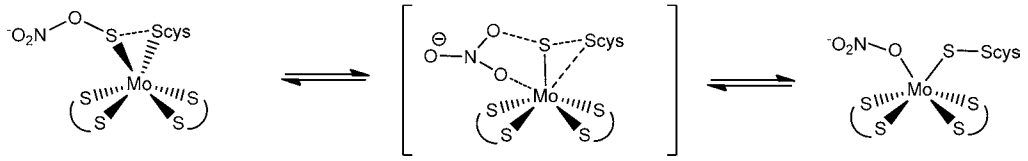

should correspond to the last step before decoordination of the cysteine residue. Electronic properties calculations were performed on the optimized geometry of model **5** for the +IV to +VI formal oxidation state. Figure 3 shows Mayer's bond

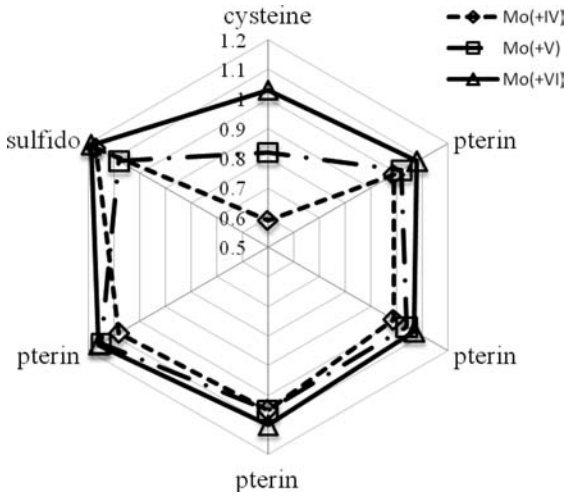

Figure 3. Mayer's bond order for the Mo−S bond in the optimized structure of model **5**.

order[89] of the various Mo−S bonds as a function of the formal valence of the metal. One can notice that all Mo−S bond indexes correspond to single bonds (value close to one) except in the case of the cysteine sulfur with a value of 0.6 for Mo(IV) and 0.8 for Mo(V). Moreover, we observed a significant increase of the partial disulfide bond index when the molybdenum is reduced (from 0.1 for Mo(VI) to 0.5 for Mo(IV)). Since Mayer's bond order is a good indicator of the strength of a coordination bond, we deduce that the more the molybdenum is oxidized, the stronger the Mo−S_{cys} bond is. Consequently, the reduced state has the longer Mo−S_{cys} bond: 2.478 Å for Mo(VI), 2.576 Å for Mo(V), and 2.747 Å for Mo(IV). We then suggest that for high oxidation states the strength of the Mo−S_{cys} bond should preclude direct approach of the substrate to the metal. Considering the hypothesis that substrate binding needs the rupture of the Mo−S_{cys} bond, this explain (i) the irreversible activation of the "high-*g* resting" species which requires in the first step a reduction of the molybdenum center in the +IV oxidation state followed by a second irreversible step,[10] which could correspond to structural changes occurring beyond the first coordination sphere of the Mo ion, (ii) the substrate binding step of the catalytic cycle on the Mo(IV) where dissociation of the cysteine ligand leads to formation of a persulfido−cysteine intermediate (Scheme 7) with an empty coordination site for the substrate approach.

The catalytic relevance of "high-*g* nitrate" and "high-*g* turnover" species remains unclear. Depending on the role of the Mo−S_{cys} breaking step, one can imagine the two following hypothesis: (a) all three "high-*g*" species correspond to catalytically inactive forms of the active site because of the strong Mo−S_{cys} bond in the +V oxidation state, (b) each "high-*g*" species can be catalytically active or not by reduction in the +IV oxidation state depending on structural arrangements beyond the first molybdenum coordination sphere.

In *Pp* NapAB and *Dd* NapA samples "very high-*g*" signals have been observed after cyanide treatment, suggesting that they are not catalytically relevant.[30,58] Since there is no disulfide bond in this species, no "sulfur-shift" mechanism can occur. In this case, the strong negative charge of the sulfido ligand could prevent approach of the nitrate anion due to electronic repulsion. Moreover, the Mo−S bond with the sulfido ligand is very strong (Mayer's bond order of 1.6). This result means that substitution of a S^{2-} ligand by the substrate, independently of the underlying steps of the nitrate reduction, appears to be very unfavorable from a thermodynamic point of view. In fact, "very high-*g*" species can be an inactive form as removal of the sulfido ligand needs too much energy.

4. CONCLUSIONS

This work provides magneto-structural correlations for the molybdenum cofactor of periplasmic nitrate reductases. The characteristic ***g*** and ***A*** tensors of Mo(V) signatures allow an accurate prediction of structural properties around the metallic center. Considering theoretical calculations of EPR parameters on simplified models, we propose structures for the active site of EPR-detected species "high-*g*", "very high-*g*", and "low-*g*" signals. While the latter seems to be a partially decoordinated state which resembles the sulfite oxidase active site, the former possess a six-sulfur coordination sphere. We suggest a strong similarity between the major "high-*g*" species and the crystal structures proposed recently for *Desulfovibrio desulfuricans* NapA[30] and *Cupriavidus necator* NapAB.[26] Whereas the catalytic relevance of EPR-detected species remains elusive, "high-*g*" and "very high-*g*" signals do not correspond to irreversibly damaged structures in the vicinity of the molybdenum ion. The disulfide bond hypothesis offers a good explanation for the inactivity of "high-*g*" states since the substrate cannot access the metal in the Mo(V) state. Reduction of the molybdenum ion weakens the Mo−S_{cys} bond and can play a crucial role in the activation process or in the catalytic mechanism. In order to have better insights into the catalytic Mo(V) states, time-resolved spectroscopies are in progress to trap and characterize catalytic intermediates. Theoretical results presented in this work used adapted structural constraints based on the crystallographic structure to mimic the protein environment; complementary studies will be made using the combined quantum mechanical/molecular mechanical (QM/MM) approaches. QM/MM methods take into account the surrounding environment and have demonstrated a good ability to model active sites of some metalloenzymes.[22,90−99]

■ ASSOCIATED CONTENT

Supporting Information

Basis set details; calculation results on well-known five- and six-coordinated molybdenum complexes for testing robustness of

dx.doi.org/10.1021/ic201533p | *Inorg. Chem.* 2012, 51, 3409−3419

the method; calculation results on the optimized structure of models **1**−**6**; calculated *g* values for the partially optimized model $\mathbf{2O}^{2-}$ with a fixed Bailar angle; calculation results on tris-dithiolene Mo(V) models; coordinates files for the best model structures (model "**4_2v3v**", model "$\mathbf{2S}^{2-}$**_2v3v**", models **7** and **9**) in *XYZ* format; angular variations of the ethanethiolate group and ^{1}H *hfc* values for models "**4_2v3v**" and "$\mathbf{2S}^{2-}$**_2v3v**". This material is available free of charge via the Internet at http://pubs.acs.org.

AUTHOR INFORMATION

Corresponding Author

*Phone: +33 4 91164559. E-mail: fbiaso@imm.cnrs.fr.

Notes

The authors declare no competing financial interest.

ACKNOWLEDGMENTS

We thank Dr. Emilien Etienne for EPR spectrum simulations and Pr. Nicolas Ferré for his help in computational aspects. All calculations were performed using the Centre Régional de Compétences en Modélisation Moléculaire (CRCMM) computing resources (Marseille). This work was funded by the "Centre National de la Recherche Scientifique", the Agence Nationale pour la Recherche (MC2 project), and the Aix-Marseille University.

REFERENCES

(1) Hille, R. *Chem. Rev.* **1996**, *96* (7), 2757−2816.
(2) Dobbek, H. *Coord. Chem. Rev.* **2011**, *255* (9−10), 1104−1116.
(3) Romao, M. J. *Dalton Trans.* **2009**, *21*, 4053−4068.
(4) Moura, J. J. G.; Brondino, C. D.; Trincao, J.; Romao, M. J. *J. Biol. Inorg. Chem.* **2004**, *9* (7), 791−799.
(5) Brondino, C. D.; Romao, M. J.; Moura, I.; Moura, J. J. G. *Curr. Opin. Chem. Biol.* **2006**, *10* (2), 109−114.
(6) Feng, C. J.; Tollin, G.; Enemark, J. H. *BBA-Proteins Proteomics* **2007**, *1774* (5), 527−539.
(7) Johnson-Winters, K.; Tollin, G.; Enemark, J. H. *Biochemistry* **2010**, *49* (34), 7242−7254.
(8) Brondino, C. D.; Rivas, M. G.; Romao, M. J.; Moura, J. J. G.; Moura, I. *Acc. Chem. Res.* **2006**, *39* (10), 788−796.
(9) Arnoux, P.; Sabaty, M.; Alric, J.; Frangioni, B.; Guigliarelli, B.; Adriano, J. M.; Pignol, D. *Nat. Struct. Biol.* **2003**, *10* (11), 928−934.
(10) Fourmond, V.; Burlat, B.; Dementin, S.; Arnoux, P.; Sabaty, M.; Boiry, S.; Guigliarelli, B.; Bertrand, P.; Pignol, D.; Leger, C. *J. Phys. Chem. B* **2008**, *112* (48), 15478−15486.
(11) Correia, C.; Besson, S.; Brondino, C. D.; Gonzalez, P. J.; Fauque, G.; Lampreia, J.; Moura, I.; Moura, J. J. G. *J. Biol. Inorg. Chem.* **2008**, *13* (8), 1321−1333.
(12) Field, S. J.; Thornton, N. P.; Anderson, L. J.; Gates, A. J.; Reilly, A.; Jepson, B. J. N.; Richardson, D. J.; George, S. J.; Cheesman, M. R.; Butt, J. N. *Dalton Trans.* **2005**, No. 21, 3580−3586.
(13) Rothery, R. A.; Bertero, M. G.; Cammack, R.; Palak, M.; Blasco, F.; Strynadka, N. C. J.; Weiner, J. H. *Biochemistry* **2004**, *43* (18), 5324−5333.
(14) Jormakka, M.; Richardson, D.; Byrne, B.; Iwata, S. *Struct. Fold. Des.* **2004**, *12* (1), 95−104.
(15) Bertero, M. G.; Rothery, R. A.; Palak, M.; Hou, C.; Lim, D.; Blasco, F.; Weiner, J. H.; Strynadka, N. C. J. *Nat. Struct. Biol.* **2003**, *10* (9), 681−687.
(16) Rothery, R. A.; Blasco, F.; Weiner, J. H. *Biochemistry* **2001**, *40* (17), 5260−5268.
(17) Blasco, F.; Guigliarelli, B.; Magalon, A.; Asso, M.; Giordano, G.; Rothery, R. A. *Cell. Mol. Life Sci.* **2001**, *58* (2), 179−193.
(18) George, G. N.; Bray, R. C.; Morpeth, F. F.; Boxer, D. H. *Biochem. J.* **1985**, *227* (3), 925−931.
(19) Hofmann, M. *J. Biol. Inorg. Chem.* **2009**, *14* (7), 1023−1035.
(20) Cerqueira, N.; Gonzalez, P. J.; Brondino, C. D.; Romao, M. J.; Romao, C. C.; Moura, I.; Moura, J. J. G. *J. Comput. Chem.* **2009**, *30* (15), 2466−2484.
(21) Jepson, B. J. N.; Mohan, S.; Clarke, T. A.; Gates, A. J.; Cole, J. A.; Butler, C. S.; Butt, J. N.; Hemmings, A. M.; Richardson, D. J. *J. Biol. Chem.* **2007**, *282* (9), 6425−6437.
(22) Leopoldini, M.; Russo, N.; Toscano, M.; Dulak, M.; Wesolowski, T. A. *Chem.—Eur. J.* **2006**, *12* (9), 2532−2541.
(23) Thapper, A.; Deeth, R. J.; Nordlander, E. *Inorg. Chem.* **2002**, *41* (25), 6695−6702.
(24) Simpson, P. J. L.; McKinzie, A. A.; Codd, R. *Biochem. Biophys. Res. Commun.* **2010**, *398* (1), 13−18.
(25) Dias, J. M.; Than, M. E.; Humm, A.; Huber, R.; Bourenkov, G. P.; Bartunik, H. D.; Bursakov, S.; Calvete, J.; Caldeira, J.; Carneiro, C.; Moura, J. J. G.; Moura, I.; Romao, M. J. *Struct. Fold. Des.* **1999**, *7* (1), 65−79.
(26) Coelho, C.; González, P. J.; Moura, J. J. G.; Moura, I.; Trincão, J.; Romão, M. J. *J. Mol. Biol.* **2011**, *408* (5), 932−948.
(27) Jepson, B. J. N.; Marietou, A.; Mohan, S.; Cole, J. A.; Butler, C. S.; Richardson, D. J. *Biochem. Soc. Trans.* **2006**, *34*, 122−126.
(28) Berks, B. C.; Richardson, D. J.; Robinson, C.; Reilly, A.; Aplin, R. T.; Ferguson, S. J. *Eur. J. Biochem.* **1994**, *220* (1), 117−124.
(29) Siddiqui, R. A.; Warneckeeberz, U.; Hengsberger, A.; Schneider, B.; Kostka, S.; Friedrich, B. *J. Bacteriol.* **1993**, *175* (18), 5867−5876.
(30) Najmudin, S.; Gonzalez, P. J.; Trincao, J.; Coelho, C.; Mukhopadhyay, A.; Cerqueira, N.; Romao, C. C.; Moura, I.; Moura, J. J. G.; Brondino, C. D.; Romao, M. J. *J. Biol. Inorg. Chem.* **2008**, *13* (5), 737−753.
(31) Bertrand, P.; Frangioni, B.; Dementin, S.; Sabaty, M.; Arnoux, P.; Guigliarelli, B.; Pignol, D.; Leger, C. *J. Phys. Chem. B* **2007**, *111* (34), 10300−10311.
(32) Cao, H.; Pauff, J. M.; Hille, R. *J. Biol. Chem.* **2010**, *285* (36), 28044−28053.
(33) Frisch, M. J.; Trucks, G. W.; Schlegel, H. B.; Scuseria, G. E.; Robb, M. A.; Cheeseman, J. R.; Montgomery Jr, J. A.; Vreven, T.; Kudin, K. N.; Burant, J. C.; Millam, J. M.; Iyengar, S. S.; Tomasi, J.; Barone, V.; Mennucci, B.; Cossi, M.; Scalmani, G.; Rega, N.; Petersson, G. A.; Nakatsuji, H.; Hada, M.; Ehara, M.; Toyota, K.; Fukuda, R.; Hasegawa, J.; Ishida, M.; Nakajima, T.; Honda, Y.; Kitao, O.; Nakai, H.; Klene, M.; Li, X.; Knox, J. E.; Hratchian, H. P.; Cross, J. B.; Bakken, V.; Adamo, C.; Jaramillo, J.; Gomperts, R.; Stratmann, R. E.; Yazyev, O.; Austin, A. J.; Cammi, R.; Pomelli, C.; Ochterski, J. W.; Ayala, P. Y.; Morokuma, K.; Voth, G. A.; Salvador, P.; Dannenberg, J. J.; Zakrzewski, V. G.; Dapprich, S.; Daniels, A. D.; Strain, M. C.; Farkas, O.; Malick, D. K.; Rabuck, A. D.; Raghavachari, K.; Foresman, J. B.; Ortiz, J. V.; Cui, Q.; Baboul, A. G.; Clifford, S.; Cioslowski, J.; Stefanov, B. B.; Liu, G.; Liashenko, A.; Piskorz, P.; Komaromi, I.; Martin, R. L.; Fox, D. J.; Keith, T.; Al-Laham, M. A.; Peng, C. Y.; Nanayakkara, A.; Challacombe, M.; Gill, P. M. W.; Johnson, B.; Chen, W.; Wong, M. W.; Gonzales, C.; Pople, J. A. *Gaussian03*, E.01; Gaussian Inc.: Wallingford, CT, 2004.
(34) Becke, A. D. *J. Chem. Phys.* **1993**, *98* (7), 5648−5652.
(35) Lee, C. T.; Yang, W. T.; Parr, R. G. *Phys. Rev. B* **1988**, *37* (2), 785−789.
(36) The SDD basis set is the combination of the Dunning/Huzinaga double-ζ basis set on lighter elements with the Stuttgart−Dresden relativistic effective core potential on heavier elements. To improve the accuracy of the calculation, the d function was added to all sulfur atoms as polarization functions (d coefficients of the 6-311g(d,p) basis set).
(37) Waller, M. P.; Braun, H.; Hojdis, N.; Buhl, M. *J. Chem. Theory Comput.* **2007**, *3* (6), 2234−2242.
(38) Neese, F. *Orca-An ab initio, DFT and semiempirical SCF-MO package*, version 2.7-0; Max-Planck Institut für Bioanorganische Chemie: Mülheim, Germany, 2010.
(39) Neese, F. *J. Chem. Phys.* **2001**, *115* (24), 11080−11096.
(40) van Wullen, C. *J. Chem. Phys.* **1998**, *109* (2), 392−399.
(41) vanLenthe, E.; Snijders, J. G.; Baerends, E. J. *J. Chem. Phys.* **1996**, *105* (15), 6505−6516.

(42) Pantazis, D. A.; Chen, X. Y.; Landis, C. R.; Neese, F. *J. Chem. Theory Comput.* **2008**, *4* (6), 908−919.
(43) Ahlrichs, R. Unpublished results.
(44) Grimme, S.; Antony, J.; Ehrlich, S.; Krieg, H. *J. Chem. Phys.* **2010**, *132*, 154104.
(45) Hernandez-Marin, E.; Seth, M.; Ziegler, T. *Inorg. Chem.* **2010**, *49* (4), 1566−1576.
(46) Neese, F. *Coord. Chem. Rev.* **2009**, *253* (5−6), 526−563.
(47) Hrobarik, P.; Malkina, O. L.; Malkin, V. G.; Kaupp, M. *Chem. Phys.* **2009**, *356* (1−3), 229−235.
(48) Hadt, R. G.; Nemykin, V. N.; Olsen, J. G.; Basu, P. *Phys. Chem. Chem. Phys.* **2009**, *11* (44), 10377−10384.
(49) Drew, S. C.; Young, C. G.; Hanson, G. R. *Inorg. Chem.* **2007**, *46* (7), 2388−2397.
(50) Neese, F. *J. Chem. Phys.* 2005, *122*, (3).
(51) Patchkovskii, S.; Schreckenbach, G. Calculation of EPR *g*-tensors with density functional theory. In *Calculation of NMR and EPR properties*; Kaupp, M., Bühl, M., Malkin, V. G., Eds.; Wiley-VCH Verlag GmbH and Co. KGaA: Weinheim, 2004; pp 505−532.
(52) Drew, S. C.; Hanson, G. R. *Inorg. Chem.* **2009**, *48* (5), 2224−2232.
(53) Fritscher, J.; Hrobarik, P.; Kaupp, M. *J. Phys. Chem. B* **2007**, *111* (17), 4616−4629.
(54) Fritscher, J.; Hrobarik, P.; Kaupp, M. *Inorg. Chem.* **2007**, *46* (20), 8146−8161.
(55) Bertrand, P.; Gayda, J. P. *Biochim. Biophys. Acta* **1979**, *579* (1), 107−121.
(56) Bertrand, P.; Guigliarelli, B.; Gayda, J. P.; Beardwood, P.; Gibson, J. F. *Biochim. Biophys. Acta* **1985**, *831* (2), 261−266.
(57) Kikuchi, T.; Sugiura, Y.; Tanaka, H. *Inorg. Chim. Acta, Bioinorg. Chem.* **1982**, *66* (1), L5−L8.
(58) Bennett, B.; Berks, B. C.; Ferguson, S. J.; Thomson, A. J.; Richardson, D. J. *Eur. J. Biochem.* **1994**, *226* (3), 789−798.
(59) Dementin, S.; Arnoux, P.; Frangioni, B.; Grosse, S.; Leger, C.; Burlat, B.; Guigliarelli, B.; Sabaty, M.; Pignol, D. *Biochemistry* **2007**, *46* (34), 9713−9721.
(60) Fourmond, V.; Burlat, B.; Dementin, S.; Sabaty, M.; Arnoux, P.; Etienne, E.; Guigliarelli, B.; Bertrand, P.; Pignol, D.; Leger, C. *Biochemistry* **2010**, *49* (11), 2424−2432.
(61) Butler, C. S.; Charnock, J. M.; Bennett, B.; Sears, H. J.; Reilly, A. J.; Ferguson, S. J.; Garner, C. D.; Lowe, D. J.; Thomson, A. J.; Berks, B. C.; Richardson, D. J. *Biochemistry* **1999**, *38* (28), 9000−9012.
(62) personal communication.
(63) Gonzalez, P. J.; Rivas, M. G.; Brondino, C. D.; Bursakov, S. A.; Moura, I.; Moura, J. J. G. *J. Biol. Inorg. Chem.* **2006**, *11* (5), 609−616.
(64) Butler, C. S.; Fairhurst, S. A.; Ferguson, S. J.; Thomson, A. J.; Berks, B. C.; Richardson, D. J.; Lowe, D. J. *Biochem. J.* **2002**, *363*, 817−823.
(65) Our attempt to obtain an optimized geometry of a model with protonation of the thiolate functions of the two pterins failed. Moreover, protonation of the two thiolate functions of the same pterin leads to its total decoordination. Only model 3 gave an optimized protonated structure with two coordinated pterins.
(66) Gangeswaran, R.; Lowe, D. J.; Eady, R. R. *Biochem. J.* **1993**, *289*, 335−342.
(67) Jepson, B. J. N.; Anderson, L. J.; Rubio, L. M.; Taylor, C. J.; Butler, C. S.; Flores, E.; Herrero, A.; Butt, J. N.; Richardson, D. J. *J. Biol. Chem.* **2004**, *279* (31), 32212−32218.
(68) Barber, M. J.; May, H. D.; Ferry, J. G. *Biochemistry* **1986**, *25* (25), 8150−8155.
(69) Rivas, M. G.; Gonzalez, P. J.; Brondino, C. D.; Moura, J. J. G.; Moura, I. *J. Inorg. Biochem.* **2007**, *101* (11−12), 1617−1622.
(70) Five coordinated complexes can have a g_{min} value of 1.98 or more, but corresponding *g* tensors are strongly axial.
(71) Bailar, J. C. *J. Inorg. Nuclear Chem.* **1958**, *8*, 165−175.
(72) Vancoillie, S.; Pierloot, K. *Theor. Chem. Acc.* **2009**, *124* (3−4), 251−259.
(73) Ryde, U.; Schulzke, C.; Starke, K. *J. Biol. Inorg. Chem.* **2009**, *14* (7), 1053−1064.
(74) Joshi, H. K.; Enemark, J. H. *J. Am. Chem. Soc.* **2004**, *126* (38), 11784−11785.
(75) Tenderholt, A. L.; Szilagyi, R. K.; Holm, R. H.; Hodgson, K. O.; Hedman, B.; Solomon, E. I. *Inorg. Chem.* **2008**, *47* (14), 6382−6392.
(76) Kaupp, M. *Angew. Chem., Int. Ed.* **2004**, *43* (5), 546−549.
(77) Mtei, R. P.; Lyashenko, G.; Stein, B.; Rubie, N.; Hille, R.; Kirk, M. L. *J. Am. Chem. Soc.* **2011**, *133* (25), 9762−9774.
(78) McNaughton, R. L.; Lim, B. S.; Knottenbelt, S. Z.; Holm, R. H.; Kirk, M. L. *J. Am. Chem. Soc.* **2008**, *130* (14), 4628−4636.
(79) Blow, D. M. *Acta Crystallogr. Sect. D: Biol. Crystallogr.* **2002**, *58*, 792−797.
(80) Torrent, M.; Vreven, T.; Musaev, D. G.; Morokuma, K.; Farkas, O.; Schlegel, H. B. *J. Am. Chem. Soc.* **2002**, *124* (2), 192−193.
(81) Prisner, T.; Lyubenova, S.; Atabay, Y.; MacMillan, F.; Kroger, A.; Klimmek, O. *J. Biol. Inorg. Chem.* **2003**, *8* (4), 419−426.
(82) Burgmayer, S. J. N. *Dithiolenes in Biology*; John Wiley and Sons: Hoboken, NJ, 2004; Vol. *52*, pp 491−538.
(83) Model ***5 SH***$^-$ is not considered here since it possesses a large *hfc* interaction with the exchangeable proton which is not observed in experimental spectra.
(84) Gutteridge, S.; Tanner, S. J.; Bray, R. C. *Biochem. J.* **1978**, *175* (3), 869−878.
(85) Hernandez-Marin, E.; Ziegler, T. *Inorg. Chem.* **2009**, *48* (4), 1323−1333.
(86) Astashkin, A. V.; Raitsimring, A. M.; Feng, C. J.; Johnson, J. L.; Rajagopalan, K. V.; Enemark, J. H. *J. Am. Chem. Soc.* **2002**, *124* (21), 6109−6118.
(87) Astashkin, A. V.; Mader, M. L.; Pacheco, A.; Enemark, J. H.; Raitsimring, A. M. *J. Am. Chem. Soc.* **2000**, *122* (22), 5294−5302.
(88) Xie, H. J.; Cao, Z. X. *Organometallics* **2010**, *29* (2), 436−441.
(89) Mayer, I. *Chem. Phys. Lett.* **1983**, *97* (3), 270−274.
(90) Greco, C.; Silakov, A.; Bruschi, M.; Ryde, U.; De Gioia, L.; Lubitz, W. *Eur. J. Inorg. Chem.* **2011**, *7*, 1043−1049.
(91) Radoul, M.; Sundararajan, M.; Potapov, A.; Riplinger, C.; Neese, F.; Goldfarb, D. *Phys. Chem. Chem. Phys.* **2010**, *12* (26), 7276−7289.
(92) Dieterich, J. M.; Werner, H. J.; Mata, R. A.; Metz, S.; Thiel, W. *J. Chem. Phys.* **2010**, *132* (3), 10.
(93) Senn, H. M.; Thiel, W. *Angew. Chem., Int. Ed.* **2009**, *48* (7), 1198−1229.
(94) Metz, S.; Wang, D. Q.; Thiel, W. *J. Am. Chem. Soc.* **2009**, *131* (13), 4628−4640.
(95) Metz, S.; Thiel, W. *J. Am. Chem. Soc.* **2009**, *131* (41), 14885−14902.
(96) Senn, H. M.; Thiel, W. *Curr. Opin. Chem. Biol.* **2007**, *11* (2), 182−187.
(97) Sinnecker, S.; Neese, F. *J. Comput. Chem.* **2006**, *27* (12), 1463−1475.
(98) Schoneboom, J. C.; Neese, F.; Thiel, W. *J. Am. Chem. Soc.* **2005**, *127* (16), 5840−5853.
(99) Moon, S.; Patchkovskii, S.; Salahub, D. R. *THEOCHEM: J. Mol. Struct.* **2003**, *632*, 287−295.
(100) Lamy, M. T.; Gutteridge, S.; Bray, R. C. *Biochem. J.* **1980**, *185* (2), 397−403.
(101) Drew, S. C.; Reijerse, E.; Quentmeier, A.; Rother, D.; Friedrich, C. G.; Lubitz, W. *Inorg. Chem.* **2011**, *50* (2), 409−411.
(102) Hemann, C.; Hood, B. L.; Fulton, M.; Hansch, R.; Schwarz, G.; Mendel, R. R.; Kirk, M. L.; Hille, R. *J. Am. Chem. Soc.* **2005**, *127* (47), 16567−16577.
(103) Stoll, S.; Schweiger, A. *J. Magn. Reson.* **2006**, *178* (1), 42−55.